Thermal fluid flow transport characteristics in nanofluid jet array impingement

Caner Senkal[1], Shuichi Torii[1,*]

[1]Department of Mechanical Engineering, Kumamoto University, Kumamoto, Japan
*corresponding author: torii@mech.kumamoto-u.ac.jp

Abstract Impinging jets have received considerable attention as they are able to provide large localized heat and mass transfer for many applications such as electronics cooling, annealing of metal and plastic, glass tempering, gas turbine cooling, drying of paper and textiles, food processing and so on. When the jet impacts to the target surface, it forms a very thin stagnation-zone boundary layer which offers little resistance to heat flow. Nanofluid is one of new types of fluid which has superior thermophysical properties. Employing nanofluids as a heat transport medium have significant advantages. Nanofluids have higher heat conduction rate, suspension stability due to nano-sized fine particles and reduced chance of erosion compared to micron sized of suspensions. One might expect that employment of nanofluids with superior thermophysical features can improve heat transfer capabilities of jet impingement cooling. The aim of the present study is to consider impingement thermal performance of Al_2O_3 nanofluid under multiple free jet impingement condition. Experimental and numerical approach including flow visualization is performed on thermal fluid flow transport phenomenon in jet array impingement.
Nanofluid jet array impingement revealed that an employing liquid has greater advantages than air impingement in terms of heat transfer capabilities. However some difficulties such as fluid leakage and high pumping power requirements can make liquid impingement cooling devices unsuitable in some situations. In liquid impingement under jet arrays, a utilizing nanofluid seems a good idea to enhance heat transfer capability of the employed impingement device, however, because of the some major concerns stated above, Al_2O_3–Water nanofluid would be not suitable for array impingement case.
Keywords: jet impingement, heat transfer performance, flow visualization, nanofluid

1 Introduction

An important conclusion from single phase- single jet impingement studies can be draw that the local rate of heat transfer decreases rapidly as one moves radially outward from the stagnation point to the wall jet downstream region. Multiple jets striking to the heated surface has a great potential to provide surface temperature uniform. Drainage of the spent fluid is, however, a critical issue in jet array applications. Crossflow between neighbouring jets blocks drainage of impinged jet and may cause heat transfer reduction on the heated surface.
Whelan et al. [1] designed a CPU cooler which employs de-ionized water jet arrays to cool an Intel Pentium 4 processor. They reported that a total cooling capacity of 200W is achieved for the surface area of 8.24 cm^2 while overall thermal resistance of the system is 0.18 K/W. One of their main motivation of designing jet array CPU cooler was to develop a thermal management component that can be manufactured simply and cost effectively. A multiple jet cooling device for electronic components was tested by Chien and Chang [2]. It was showed that small jet spaces result better cooling performance than larger ones. In their paper, fins are also used as jets impinged on them, to further increase cooling performance of the designed cooling device.
Jiji et al. [3] investigated a multiple jet impingement experimentally. Arrays of four or nine free surface jets are studied. Here Jet diameter was 0.5mm and 1mm. Their results revealed that with the decreasing of the spacing between the adjacent jets, the uniformity of heater surface temperature is improved. For the non-dimensional separation distance, H/D, between 3 and 5, it was observed no significant heat transfer enhancement.
Womac et al. [4] studied 2x2 and 3x3 multiple jet impingement both for free surface and submerged jet condition. Here, nozzle length was 4.78mm. Two nozzle diameters were tested, dn=0.513mm and 1.02mm. Reynolds numbers were in the range of Re=500 to 20000. Jet to target plate spaces, H/dn, was varied over the range from 5 to 10. Experiments were performed for water and a fluorocarbon liquid (FC-77). Heater block was square shaped, 12.7mmx12.7mm copper block. Results showed that for a prescribed volumetric flow rate, the largest average heat transfer coefficients correspond to arrays with the smallest

nozzle diameter and for a fixed diameter, to arrays with the smallest number of nozzles. It is also emphasized that at high flow rates of working fluid, an impacted fluid splats from the free surface near the impingement region. They stated that this effect causes average heat transfer coefficient reduction due to the bulk warming.

Pan and Webb [5] investigated heat transfer characteristics of staggered and in line arrays of free surface liquid jets. Jet to jet spacing, S/dn, ranged from two to eight in the jet Reynolds number range of 5000 to 20000. 1, 2 and 3mm nozzle diameters were tested. Dimensionless nozzle to heated surface distance, H/dn, was 2 and 5. Local heat transfer coefficient as well as central jet module averaged Nusselt number measurements are carried out by means of radiometry technique. They found that different jet configurations (in-line array and the staggered array) with different nozzle-to-nozzle spaces show no particular influence on heat transfer coefficient. Moreover Nusselt number under the central jet is independent of array configuration and jet-to-jet spacing.

Average heat transfer and pressure drop measurements were executed both for free surface and submerged multiple jet impingement by Robinson et.al. [6]. In experiments, deionized water was discharged from 1mm diameter jet holes with dimensionless jet to jet spacing, S/dn=3, 5 and 7. Dimensionless jet-to-target spaces varied between $2 \leq H/dn \leq 30$. Their measurements showed that there is a noticeable dependence of the surface average heat transfer with jet-to-target distance, H/dn. Average Nusselt number decreases with increasing H/dn. They pointed out that for the small nozzle to plate distances ($2 \leq H/dn \leq 3$), reduction of average Nusselt number with increasing H/dn attributs to the transition from submerged jet flow to free surface jet flow. Moreover, they concluded that for jet to target spaces below 10, the heat transfer coefficient results reveal the free and submerged jets are identical. A stronger dependence on jet to jet spacing was also reported for small jet to target spaces as compared with larger ones.

Heat transfer performance of microjet arrays was investigated by Fabbri et al. [7]. Test fluid was deionized water and FC-77 refrigerant. Jet diameters considered were within range of 69μm and 250μm. Jet Reynolds number varied from 73 to 3813. Only free surface jets were taken into account in experiments. Nozzle to heated surface distance was kept at 10mm constant throughout all measurements. Results showed that Nu improves with increasing Reynolds and Prandtl numbers and decreasing jet to jet spacing, S/dn.

A multiple submerged jet impingement was experimentally and numerically studied by Tie et al. [8]. It was shown that, in terms of same heat transfer coefficient obtained on the heated surface, discharged liquid velocity impinged to the heated surface is lower in larger diameter jets. In terms of same flowrate, small diameter jets gave high heat transfer rate except for the very small diameters (0.5mm and 1mm) considered in their study. Results of these very small diameters showed that adjacent jets interact to each other prior to impingement due to the short jet to jet spaces.

An experimental investigation of a 36nm Al_2O_3-water nanofluid under submerged impingement condition was carried out by Nguyen et al. [9]. Here the nanofuld was employed as the working fluid. Nanofluid in their experiments which has volume fraction up to 6% was discharged from a single 3mm diameter nozzle and impacted on a circular horizontal heated surface. Reynolds number was in the range of $3800<Re<88000$. Nozzle to heated surface separation distance was set to 2, 5 and 10mm. They stated that the dispersant agents were used in nanofluid in order to provide good particle suspension. Results showed that with regard to the nanofluid effects on surface–fluid temperature difference (ΔT) relative to a distilled water, use of nanofluids provides a lower value of ΔT. Nanofluid of the 6% volume fraction gives highest ΔT values among 2.8% and distilled water, for the case of 2, 5, 10mm separation distances. Authors stated that for small (2mm) or large (10mm) nozzle to surface distance for 36nm, Al_2O_3-water nanofluid does not provide any heat transfer enhancement. Only for an intermediate distance, 5mm, for relatively low volume fractions, 2.8%, a high heat transfer yields. Authors attributed this unfavorable heat transfer effect to two reasons: first one is due to the recirculation zones on top of the radial outward flow. Because of experiments are performed under confinement, nanofluid after impingement is entrapped in the confined channel. This effect lowers heat transfer on the heated surface due to hot, entrapped nanofluid inside recirculation zone. Second reason, for the large separation distance, i.e., increased dynamic viscosity causes low heat transfer performance, especially for the 6% volume fraction. High dynamic viscosity reduces fluid outward flow velocity and when it is combined with high recirculation zone, an unfavorable heat transfer phenomenon occurs.

Li et al. [10] investigated heat transfer features of Cu-Water nanofluid experimentally. Working fluid was discharged from 2mm single nozzle under submerged condition. Three jet-to-target distances (2, 4 and 6 mm) were studied, namely, H/D=1, 2, 3, where H/D was the ratio of jet-to-target distance H to the nozzle diameter D. 1.5%, 2.0%, 2.5% and 3.0% volume fractions of Cu-water nanofluids were tested. Reynolds number in their study was in the range of 2000 < Re < 15000. Their results showed that with respect to the same Reynolds number, Cu-water nanofluid has larger heat transfer coefficient of jet impingement than pure water. As a whole, the enhanced impingement performance of the nanofluid increases with the volume fraction of nanoparticles. For the nanofluid containing 3.0% nanoparticles volume fraction, the convective heat transfer coefficient is 52% higher in comparison with the case of pure water. They concluded that nanofluids consisting of Cu nanoparticles manifest better performance of enhanced heat transfer.

There are several numerical investigations pertinent to thermal fluid flow of Nanofluids between stationary or moving plates or through an annulus etc., a part of jet impingement configuration mentioned so far. The laminar forced convection flow of nanofluids between two coaxial and parallel disks with central axial injection was investigated by Palm.et al. [11] numerically using temperature dependent nanofluid properties. Their measurement showed that Water- Al_2O_3 nanofluid with a volume fraction of nanoparticles 4% can produce a 25% increase in the average wall heat transfer coefficient when compared to the base fluid (water) alone. Feng et al. [12] executed numerical simulations for alumina-water nanofluid flow with heat transfer between parallel disks. Their results demonstrated that nanofluids provide smoother mixture flow fields and temperature distributions.

A thorough literature review in previous section showed that the majority of the studies related to nanofluid jet impingement are conducted for submerged and single jet condition. There is no study of heat transfer characteristics of a free jet array impingement that adopted nanofluids as the working fluid. Careful experimental and numerical characterization of heat transfer of nanofluid jet array impingement is lacking in the body of literature. Also, air cooling techniques of electronic components such as coaxial air jet impingement still widely used in industry in order to provide uniform temperature gradients on device surface. The aim of the present study is to consider impingement thermal performance of Al_2O_3 nanofluid under multiple free jet impingement condition. Experimental and numerical approach including flow visualization is performed on thermal fluid flow transport phenomenon in jet array impingement.

2 Experimental apparatus and method

A schematic of the experimental test rig is shown in Fig.1 and impingement plate and nozzle assembly are illustrated in Figs. 2 and 3, respectively. Two different magnetically driven pumps are used to circulate working fluid in the system. Here Pump-1 is used to force the working fluid to the nozzle while a less capacity pump (pump-2) is utilized to drain the working fluid after impingement due to keeping impinging jets under the free surface condition. Pump-1 line is referred to as injection line while the line that pump-2 is mounted is referred to as suction line throughout this study. A by-pass line both for injection and suction lines is constructed. Former one is due to control required flow rate that excessive flow is sent back to tank trough this line. The latter one is due to keep the working fluid under desired level in the acrylic impingement. A constant temperature water bath (EYELA NCB-2200, Tokyo Rikakikai Co.) is used to control working fluid temperature at the nozzle inlet. A vortex flowmeter (Nagano Keiki Ltd. Co.,Tokyo) is mounted to monitor the flowrate of the working fluid prior entering to the nozzle plenum. Globe and Ball valves are used to control flow throughout injection and suction lines. Flexible hoses are utilized for connection purposes between pumps and water bath. Water bath has 22 liter tank that its volume is quite high for nanofluid as the working fluid in the circulation.

There are three jet holes configuration investigated in this study. Illustrations and diameters of them are shown in Fig. 2. Jet hole configuration is in radial staggered formation. Jet holes at orifice plate are drilled in a circular area same to the impingement surface (31.5 mm), that as many jet holes as possible populated within this area for the desired jet to jet spacing parameter under the staggered radial formation. For example, there are only 9 jets drilled in a 31.5mm diameter (same size with impingement surface) for S/dn =7 case, taking radial staggered formation into consideration, while there are 25 jet holes under the S/dn=3 case. Jet orifice plates are manufactured from aluminum and its thickness is 2mm. It is mounted to a brass, cylindrical plenum chamber that has 32mm inner and 80mm outer diameter. The fluid entering to jet orifice plate holes does not have enough distance to develop prior discharging toward impinging surface so it can be assumed that jets issuing from nozzles have uniform velocity profile at the nozzle tip. In order to adjust nozzle to impingement plate distance, long enough bolts are also mounted to the orifice plate with adjustment.

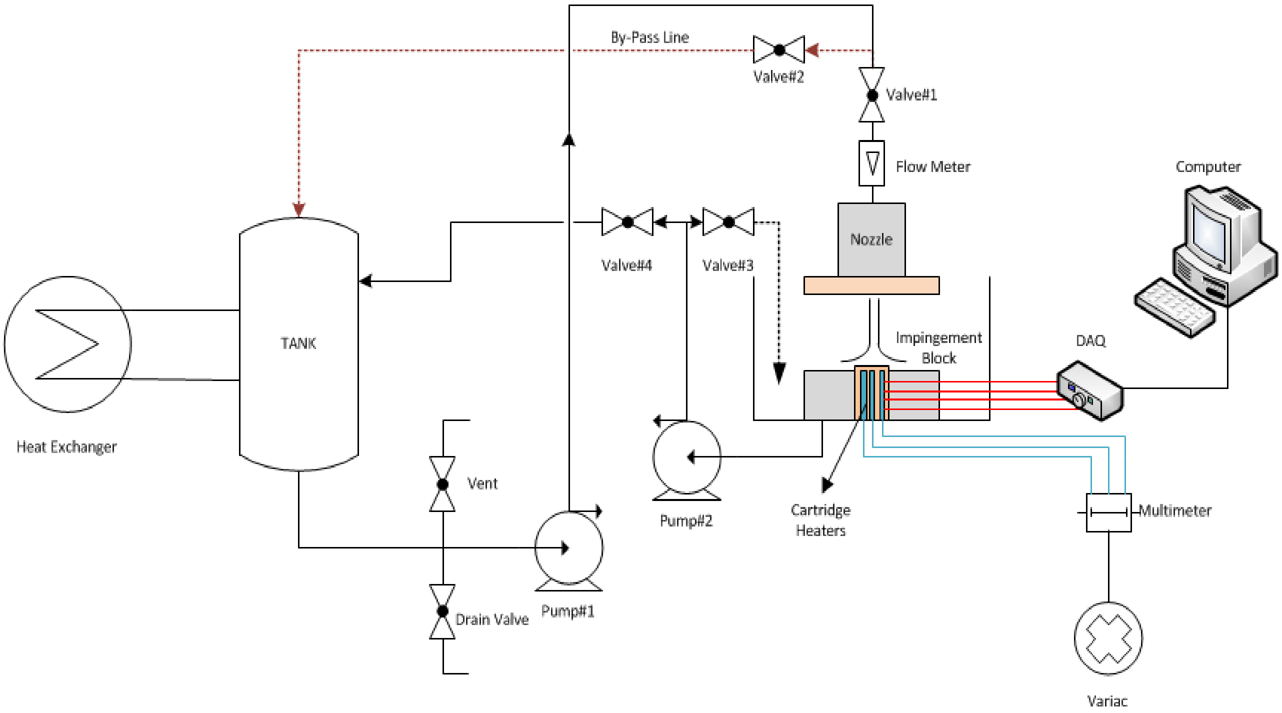

Fig. 1 Schematic of experimental apparatus

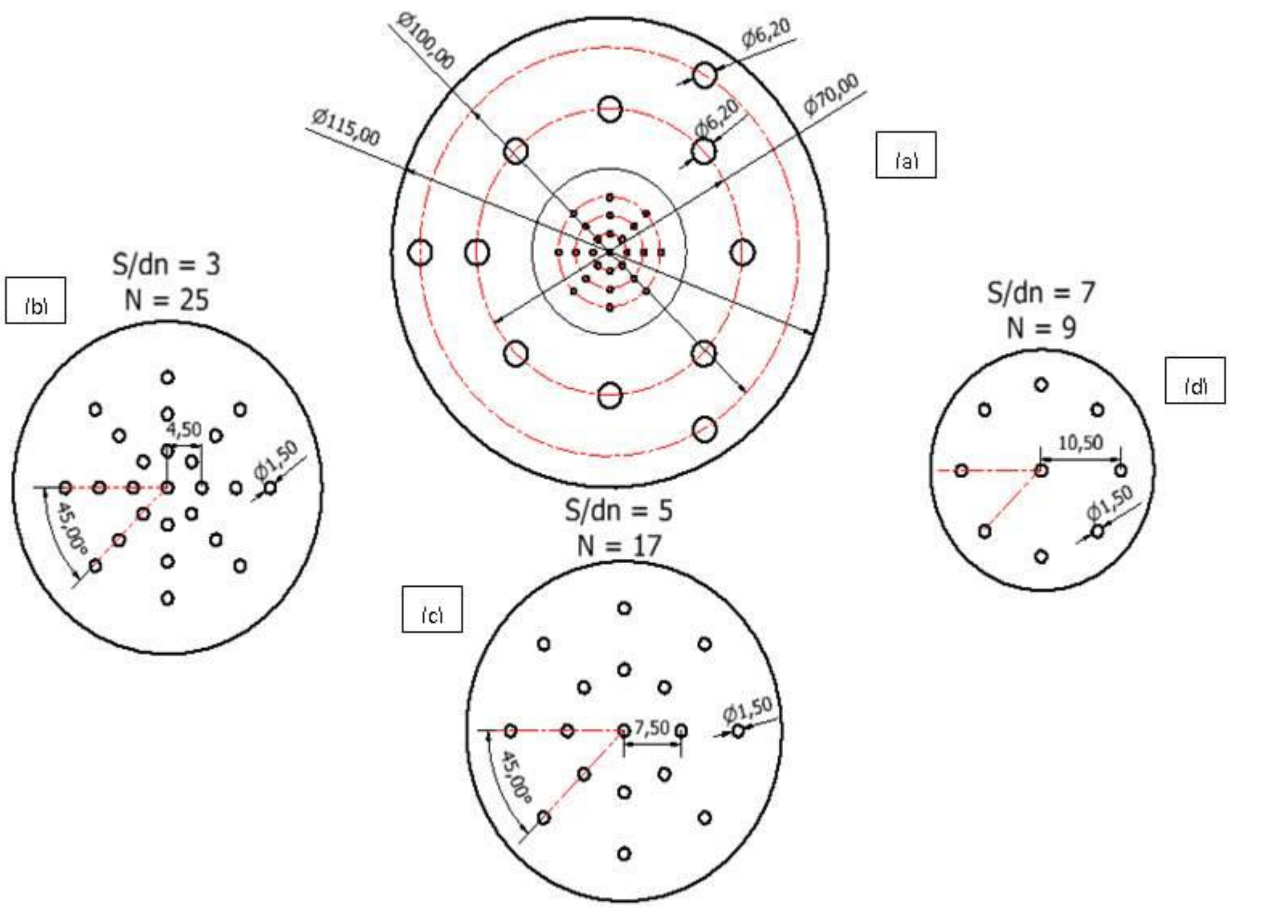

Fig. 2 Jet nozzle hole configuration. (a)whole nozzle orifice plate (b) Detail View of N=25 nozzle (c) Detail view of N=17 nozzle, (d) Detail view of N=9 nozzle

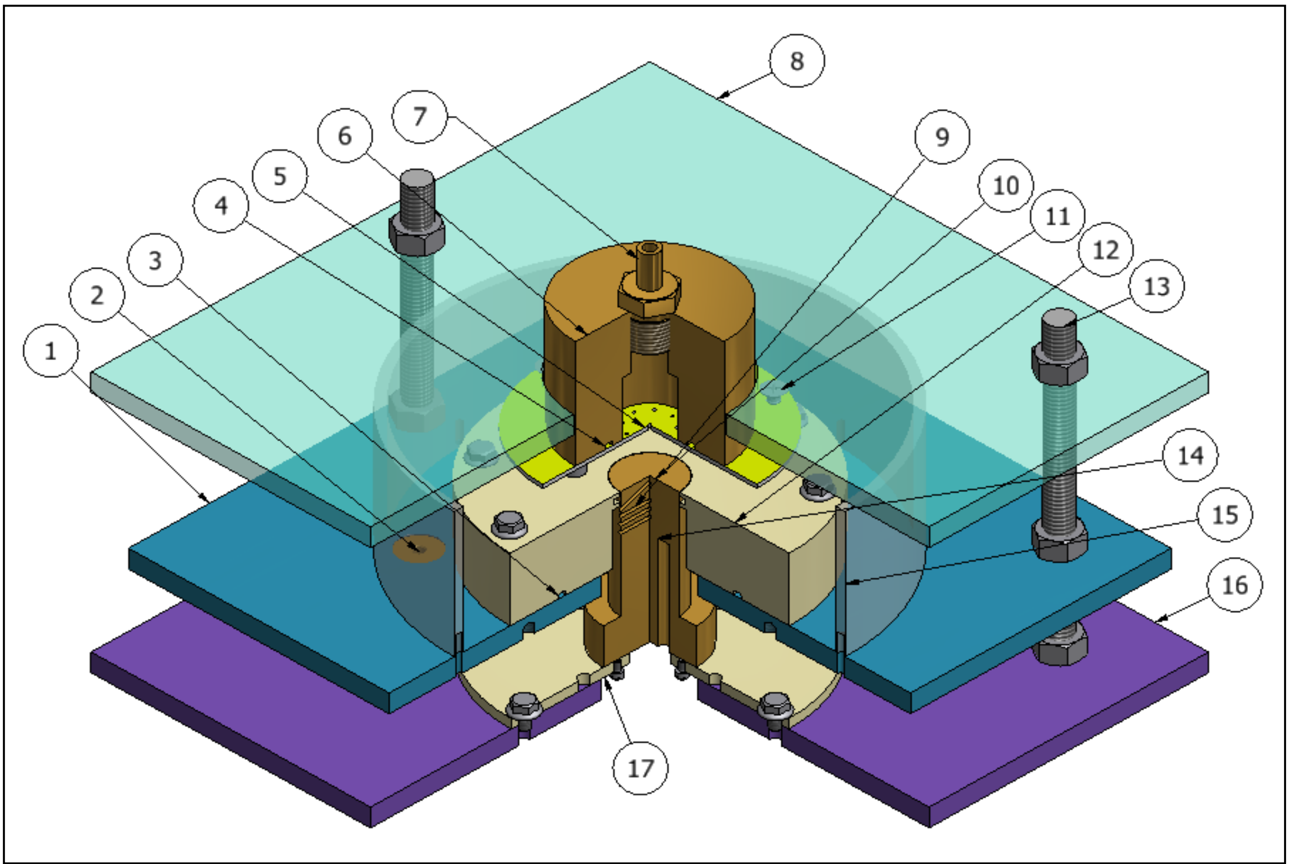

Fig. 3 Section View of Nanofluid Impingement Test Section. 1)Acrylic Base Plate, 2)Liquid Drain Hole, 3-4)O-ring Groove, 5) Interchangeable Nozzle Plate, 6) Brass Nozzle, 7) Hose Nipple Connected to Nozzle, 8) Acrylic Cover Plate, 9) Brass Impingement Block, 10) Thermocouple Holes inside Brass Impingement Block, 11) Height Adjustment Screw, 12-17)Teflon Insulation, 13)Rod, 14)Cartridge Hole Inside Impingement Block, 15) Acrylic Enclosement, 16) Acrylic Bottom Base Plate

In the present study, Al_2O_3–Water nanofluid is employed in experiments. Al_2O_3 nanoparticles with an average diameter of 31 nm are dispersed in distilled water. The nanofluids with three volume fractions, 0.5%, 2%, and 4.9% are prepared and used in experiments in order to investigate its heat transfer capability. The volume fraction φ and the required nanoparticle volume V_{np} to obtain nanoparticle suspension are defined as follows:

$$\varphi = \frac{V_{np}}{V_{bf}} \tag{1}$$

$$V_{np} = \frac{m_{np}}{\rho_{np}} \tag{2}$$

For spherical shaped nanoparticles, the formula for correlating the alumina-water nanofluid thermal conductivity, k_{nf} to the thermal conductivities of the solid nanoparticles (k_s) and base fluid (k_{bf}) developed by Maxwell [13] as follows:

$$k_{nf} = \frac{k_s + 2k_f + 2\emptyset(k_s - k_f)}{\frac{k_s}{k_f} + 2 - \emptyset(\frac{k_s}{k_f} - 1)} \tag{3}$$

Thus Maxwell's equation (3) is used in the present study to evaluate alumina-water colloid thermal conductivity.

The density ρ_{nf} of Al_2O_3 particles is determined by the nanoparticle manufacturer (CIS NanoTek) as 3500 kg/m^3 and temperature dependent water densities can be found in a standard textbook. Based on the mass equilibrium or proportional mixing principle, the density of nanofluids (ρ_{nf}) at different φ can be obtained by [14];

$$\rho_{nf} = \varphi\rho_{np} + (1-\varphi)\rho_{bf} \tag{4}$$

where ρ_{np} and ρ_{bf} are the densities of the solid nanoparticles and base fluid, respectively.
The specific heat of a nanofluid, c_{nf}, can be calculated according to [15] as:

$$c_{nf} = \emptyset\left(\frac{\rho_s}{\rho_{nf}}\right)c_s + (1-\varphi)\left(\frac{\rho_f}{\rho_{nf}}\right)c_f \tag{5}$$

The above formula as well as Eq. (5) was employed in this study.
In general, the nanofluid viscosity (μ_{bn}) increases with increasing nanoparticle volume fraction. By considering the effect due to the Brownian motion of particles, Batchelor et.al. [15] proposed as;

$$\mu_{nf} = \mu_{bf}(1 + 2.5\varphi + 6.5\varphi^2) \tag{6}$$

The above formula was used to determine the viscosity of nanofluid employed here.
Heat transfer measurements are represented for dimensionless Nusselt number. Heat transfer coefficient and Nusselt number are averaged over heated impingement surface. As mentioned previously, the top embedded thermocouple's temperature reading is utilize to asses surface heat flux and it is assumed uniform throughout the impingement surface. Average heat transfer coefficient (HTC) is defined as;

$$\bar{h} = \frac{q"}{T_s - T_j} \tag{7}$$

q" is the surface heat flux calculated from;

$$q" = k_{Br}\frac{dT}{dz}\bigg|_{Best\ Fit} \tag{8}$$

Here k_{Br} is the thermal conductivity of brass heater block. Surface temperature and nozzle exit jet temperatures are Ts and Tj, respectively. Bar over a variable represents that variable is averaged over the surface area. Average Nusselt number is defined as:

$$\overline{Nu}_{d_n} = \frac{hL_c}{k_f} \tag{9}$$

Since there is one impingement surface size considered in experiments, characteristic length Lc is taken half of the impingement surface diameter, Lc=15,75 mm. Nusselt number based on nozzle diameter also can be evaluated from equation (9), as:

$$\overline{Nu}_{L=}0.0952 \times \overline{Nu}_{d_n} \tag{10}$$

0.0952 is the coefficient divided nozzle jet diameter to half heater length as, 1.5/15.75=0.0952.
Heat transfer characteristics of a jet array impingement in terms of jet velocity can be examined by a dimensionless number, called Reynolds number. The jet Reynolds number in this study was determined from the average jet velocity calculated from the measured water flow rate. The jet velocity and thus the jet Reynolds number can then be calculated using the equations below.

$$Re_d = \frac{V_n d_n}{\nu_{film}} \tag{11}$$

$$V_n = \frac{4\dot{V}}{N\pi d_n^2} \tag{12}$$

3 Governing equations and numerical method

The proposed physical model to be studied and the coordinate system are schematically illustrated in Figs. 4 and 5. Since the flow is symmetric respect to the central jet axis, only one eighth of the geometry is taken into consideration in simulations. The following assumptions are imposed in the formulation of the problem: incompressible, steady flow; uniform inlet velocity, uniform inlet fluid temperature; and negligible axial conduction (due to the high Peclet number). Under these assumptions, the simplified governing equations for mass, momentum and energy read:
Continuity equation:

$$\frac{\partial \rho U_i}{\partial x_i} = 0 \tag{13}$$

Momentum equation:

$$\rho U_j \frac{\partial U_i}{\partial x_j} = -\frac{\partial P}{\partial x_i} + \frac{\partial}{\partial x_j}\left[\mu\left(\frac{\partial U_i}{\partial x_j} + \frac{\partial U_j}{\partial x_i}\right) - \rho\overline{u_i u_j}\right] \tag{14}$$

Energy equation:

$$c_p \rho U_i \frac{\partial T}{\partial x_i} = \frac{\partial}{\partial x_i}\left(\lambda \frac{\partial T}{\partial x_i} - c_p \rho\overline{u_i t}\right) \tag{15}$$

The Reynolds stress in Eq. (14) is obtained using the Boussinesq approximation as:

$$-\rho\overline{u_i u_j} = -\frac{2}{3}\delta_{ij}\rho k + \mu_t\left(\frac{\partial U_i}{\partial x_j} + \frac{\partial U_j}{\partial x_i}\right) \tag{16}$$

Here, the turbulent viscosity μ_t is expressed in terms of the turbulent kinetic energy k and its dissipation rate ε through the Kolmogorov-Prandtl's relation [17] as

$$\mu_t = C_\mu f_\mu \rho \frac{k^2}{\varepsilon} \tag{17}$$

$C\mu$ and $f\mu$ are a model constant and a model function, respectively. Torii et al. [18] developed a low Reynolds number version of the k-ε turbulence model capable of reproducing the transition from turbulent to laminar flows. Here the model was originally developed by Nagano and Hishida [19]. The same model [18] is employed here. Both transport equations read

$$\rho U_j \frac{\partial k}{\partial x_j} = \frac{\partial}{\partial x_j}\left[\left(\mu + \frac{\mu_t}{\sigma_k}\right)\frac{\partial k}{\partial x_j}\right] - \rho\overline{u_i u_j}\frac{\partial U_i}{\partial x_j} - \rho\varepsilon - 2\mu\left(\frac{\partial\sqrt{k}}{\partial x_j}\right)^2 \tag{18}$$

$$\rho U_j \frac{\partial \varepsilon}{\partial x_j} = \frac{\partial}{\partial x_j}\left[\left(\mu + \frac{\mu_t}{\sigma_\varepsilon}\right)\frac{\partial \varepsilon}{\partial x_j}\right] - C_1 f_1 \rho\frac{\varepsilon}{k}\overline{u_i u_j}\frac{\partial U_i}{\partial x_j} - C_2 f_2 \rho\frac{\varepsilon^2}{k} + \nu\mu_t\left(1 - f_\mu\right)\left(\frac{\partial^2 U_i}{\partial x_j^2}\right)^2 \tag{19}$$

The empirical constants and model functions in Eqs. (17), (18) and (19) are summarized in Table 1.
The turbulent heat flux in Eq. (3) can be expressed in the following form:

$$-c_p\rho\overline{u_i t} = \lambda_t\frac{\partial T}{\partial x_i} = \frac{\nu_t c_p \rho}{\mathrm{Pr}_t}\frac{\partial T}{\partial x_i} \tag{20}$$

where 0.9 is adapted as the value of Pr_t.
The height of the first cell adjacent to the wall is very important in wall bounded turbulent flow calculations. A trial and error process is conducted if the center of the first cell adjacent to the wall normal direction is in the desired y^+ range or not. The desired value of y^+ depends to the turbulence model adopted in simulations. The study of choosing the appropriate turbulence model is also performed. For the low Reynolds number turbulence models, y^+ is in the order of $y^+\approx 1$.
The flow can be assumed to obey three dimensional Navier-Stokes equations for turbulent incompressible flow in the axisymmetric coordinate system. Simulations have been performed using multiphase volume of fluid (VOF) model that liquid and air are chosen as two distinct phases. Volume of fluid is a simple multiphase model. Eulerian multiphase model is employed when defining the mixture composition. This model, which is used for both the Multiphase Segregated Flow model and the Volume of Fluid model, controls the definition of Eulerian phases within the physics continuum. It contains no Eulerian phases in its initial state. Convection and diffusion terms are discretized using 2nd order implicit scheme.
Gravity effects are also taken into account in analysis. Each distinct phase has its own set of conservation equations. Phases are considered to be mixed on length scales smaller than the length scales to resolve, and coexist everywhere in the flow domain.
Isoflux boundary conditions determined by the experiments are applied on the impingement plate. In all multiple jet computations, nozzle to heated plate distance, H/dn, is taken as 12.33 while jet to jet spaces, S/dn , is seven which corresponds to 9 jets. Nozzle length is 2mm which corresponds to discharged jet is not hydrodynamically fully developed. Outlet boundary is defined as zero pressure boundary which is located 10.5dn away from the central nozzle. Nanofluid concentrations and thermosphysical properties applied in simulations are taken from correlations, respectively.

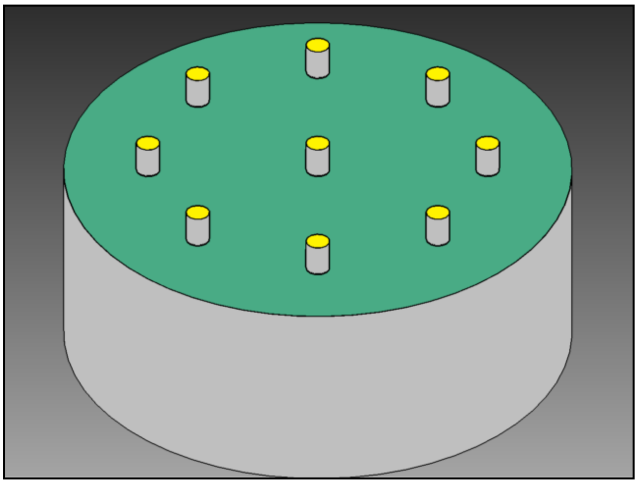

Fig.4 Top View of Whole Computational Domain for Nanofluid Impingement Simulations, S/dn=7, H/dn=12.33, and N=9

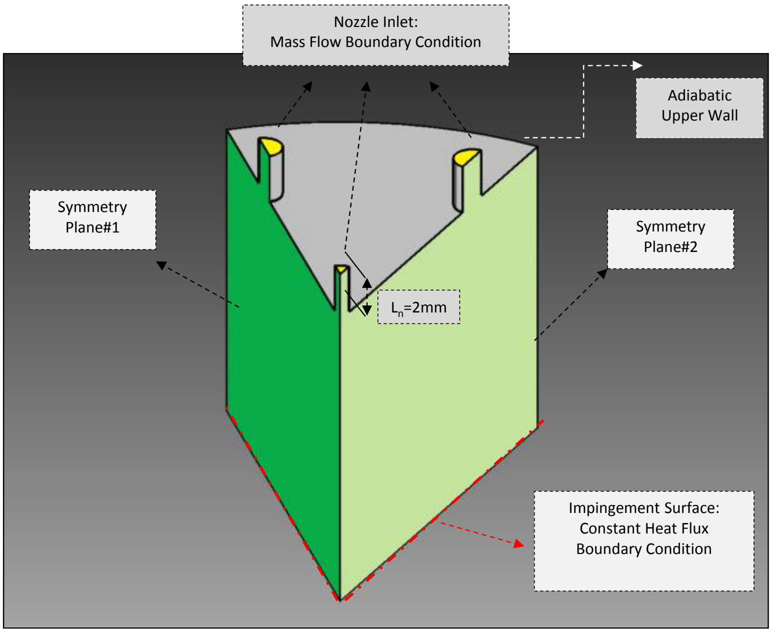

Fig. 5 One-eigth part of the computational domain, S/dn=7 and H/dn=12.33, N=9

Table 1 Empirical constants and model functions in the k-ε turbulence model

C_μ	C_1	C_2	σ_k	σ_ε	f_1	f_2	f_μ
0.09	1.44	1.9	1.0	1.3	$1+0.28\exp\left(-\frac{R_t}{25}\right)$	$1-0.3\exp(-R_t^2)$	$\left\{1-\exp\left(\frac{-R_\tau}{26.5}\right)\right\}^2$

4 Results and discussion

Figures 6(a)-(c) show Reynolds number dependency of average Nusselt number, $\overline{Nu_{d_n}}$ at H/dn=12.33 for S/dn=3,5 and 7 for various nanofluid concentrations and for pure water. For each of the working fluid considered, it is observed that an increase in Reynolds number yields high average heat transfer coefficient on the impingement surface. Such behavior is obviously due to the fact that with increasing mass flow rate, the forced convection effect also increases considerably, which in turn, augments the average heat transfer on the impingement surface in general. Thus, for a given fluid inlet temperature, the heated surface temperature would logically decrease for higher mass flow rate. Such a result has consistently been observed for water and the three nanofluids (0.5%, 2% and 4.9% of particle volume fractions) and for each of the nozzle to nozzle spaces, S/dn=3, 5 and 7. With regard to the nanofluid effects on average Nu relative to that of pure water, the results have surprisingly revealed that the use of nanofluids does not necessarily provide a higher value of average Nu. On the contrary, each nanofluid concentrations give worse cooling performance than pure water under the nearly same Reynolds number. This phenomenon was also observed by Nguyen et al. [20] for confined and submerged jet impingement case. In Nguyen et al.'s [20] study, 2.8% Al_2O_3-water nanofluid concentration gave some enhanced heat transfer rates under intermediate nozzle to impingement surface distance. They reported that using high concentrations of nanofluids for very small or large separation distances, a clear decrease of the convective heat transfer coefficient yields in comparison with that obtained using distilled water.

Location of this fluid pool is between neighboring jets. This yields a fluid circulation on the heated surface before washed away by incoming fluid jet. As the thermal conductivity of nanofluid concentration is higher than that of pure water, this entrapped liquid pool gets warm faster and thermal boundary layer inside fluid pool reaches to its fluid surface, so, this causes the heat transfer rate reduction on the impingement surface. To observe the height of this fluid pool, videos are recorded using a high speed video camera for each Reynolds number. Figures 7(a)-(g) illustrate fluid pool on the heated surface for the 2% nanofluid concentration, H/dn=12.33 and S/dn=9 for Reynolds number in the range of $1280 \leq Re_{dn} \leq 6500$. It is clear to see from images that increasing fluid velocity induces higher pool height on the surface.

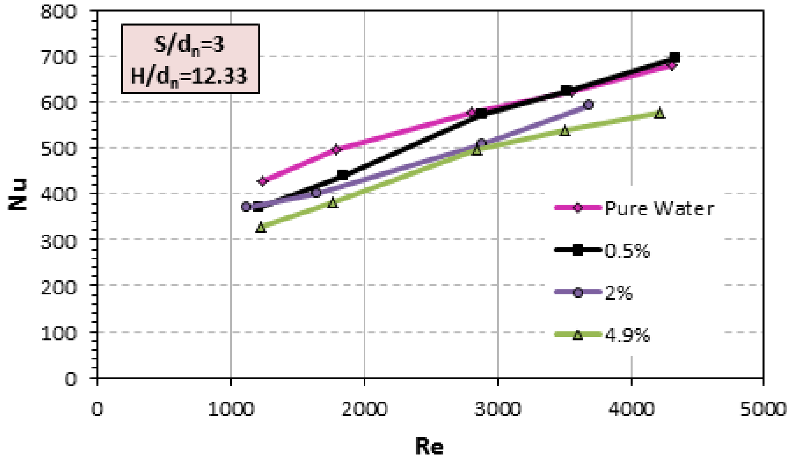

(a)

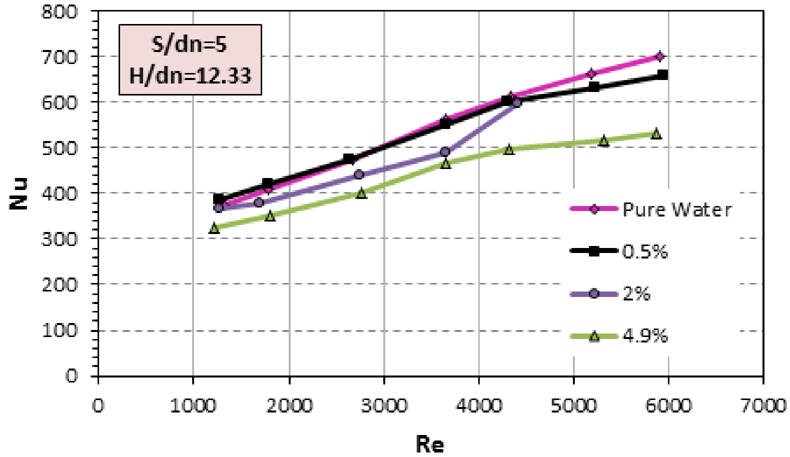

(b)

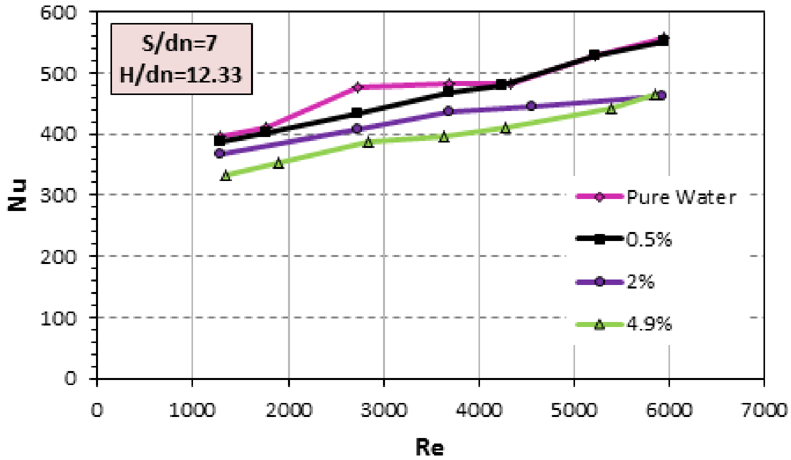

(c)

Fig. 6 Average Nusselt Number for Various Reynolds Number at nanofluid Experiments, (a) S/dn=3, (b) S/dn=5, and (c) S/dn=7

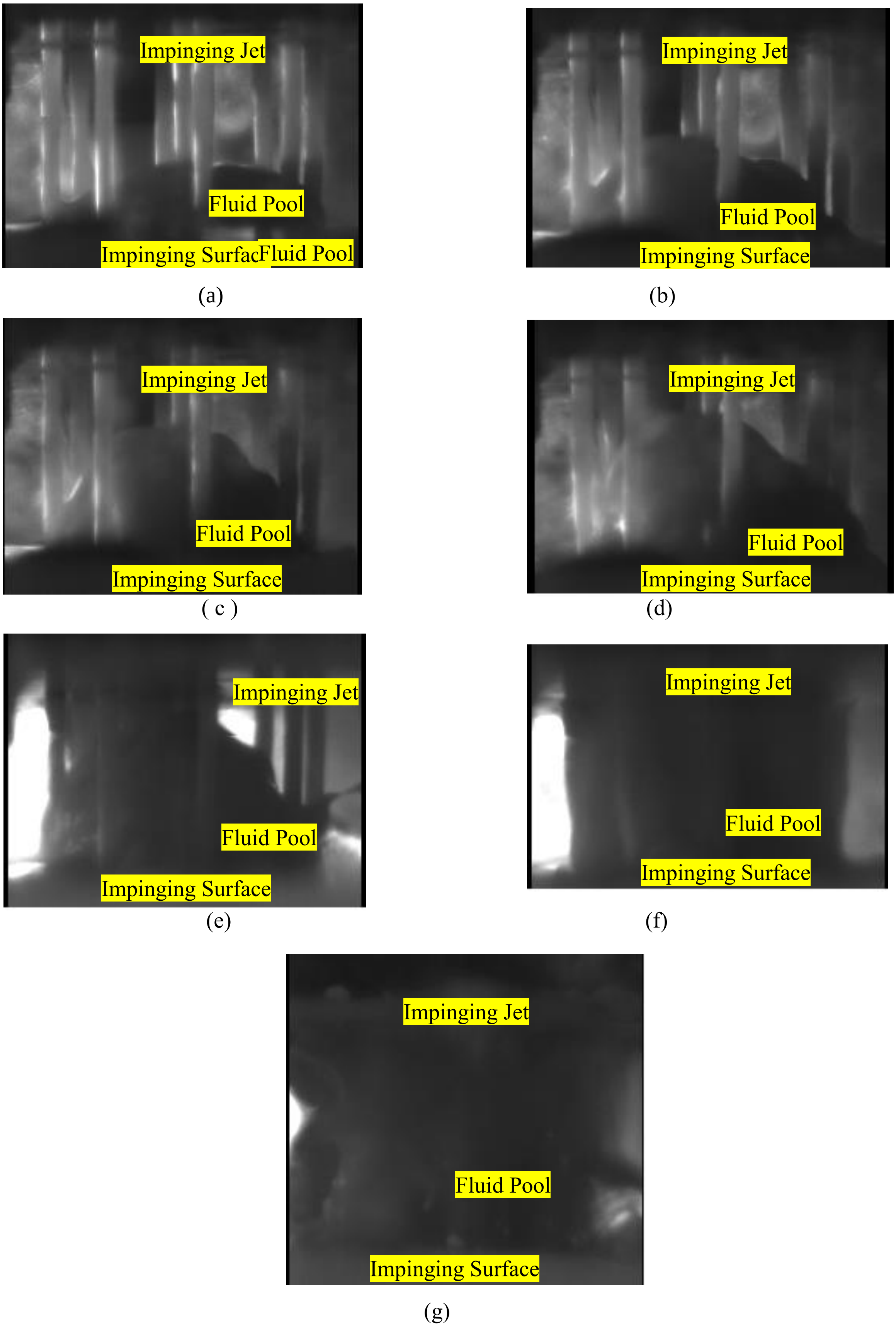

Fig. 7 Visualization of Impinging Jet Array Columns. (a)Re=1280, (b)Re=1760, (c)Re=2721, (d)Re=3681, (e)Re=4561, (f)Re=5282, and (g)Re=6500

High speed video camera images also revealed that beyond a certain Reynolds number (Re ≥ 4500) for S/dn=7, H/dn=12.33 and for the 2% nanofluid concentration, nanofluid pool height reaches to the nozzle orifice plate and significantly influences formation of discharging jet columns. As a result, a partially submerged impingement condition is formed under this situation. It is postulated that this growing nanofluid pool dramatically influences discharging jet momentum at the nozzle tip, hence the discharged jet velocity decreases by fluid fountain influence at the fluid pool which is forming towards discharging jet upstream. It is also observed that increased jet velocity at the nozzle exit at high Reynolds numbers also causes fluid splashing. The splashing of the liquid results in an attenuated film thickness on the heated surface. From visual observation of the jet arrays, it is identified that the fluid splashes away from the free surface in the vicinity of the impingement region. This phenomenon also suppresses heat transfer rate but the authors believe that this splashing phenomenon has a limited effect on heat transfer reduction due to the jet array impingement on the surface. If there is a single jet impinging on, splashing significantly effects the cooling performance because of fluid film thickness reduction on the impingement surface. There are at least 9 impinging jet columns considered in this study so the fluid film thickness reduction on the surface is a minor concern and it is not the main heat transfer reduction as oppose to the pool formation effect on the heated surface.

Figure 8 depicts experimental and numerical averaged Nusselt number results for pure water. It is observed a good agreement between Re=1765 and Re=2728 cases. For the Re=1283 case, numerical results under-predict averaged Nusselt number. In high Reynolds number cases (Re=3691 and 4333) numerical results show a monotonous average Nu increment on the plate while experimental results show a heat transfer reduction from Re=3691 to Re=4333. This reduction on experiments can be related to fluid splattering effect on the plate, which is explained in detail in the following. However, in numerical simulations, strong splattering effect is observed, but its influence on heat transfer coefficient is not significant. It is observed a continuous fluid film on the impingement surface in simulations, however in experiments, according to the physical observations, fluid film on the impingement surface in the intermediate and high Reynolds number range is not continuous at every case. This result can be the one of the reason why numerical results and experimental measurements differs each other intermediate/high Reynolds number ranges.

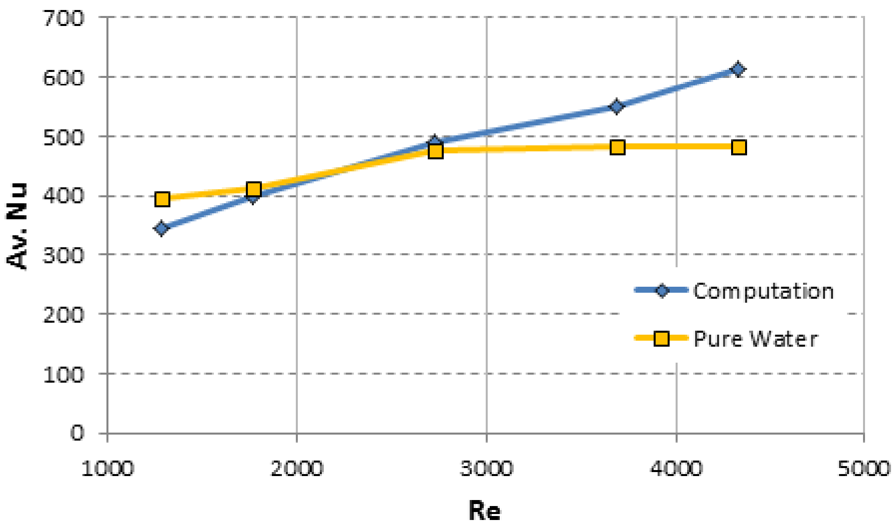

Fig. 8 Numerical Result vs Experimental Result for the case of Pure Water, H/dn=12.33, S/dn=7

Figure 9 plots numerical results along with experimental results for the φ=0.5% nanofluid suspension. As for averaged Nusselt number for the case of Re=1284, numerical computation and experimental results are in a very close agreement. As the Reynolds number increases, the difference between computations and experimental results also increase. Again, this is due to high fluid splashing effect on the heated plate. It is observed a strong fluid splattering in experiments for high Reynolds number, however, even same strong splashing phenomenon is also observed in computations and the heat transfer influence of this effect is limited in numerical analysis compared to experimental results.

Figures 10 and 11 depict average Nusselt number for φ= 2% and 4.9% respectively. Again, for the low

Reynolds number, computation and experiment results show very good agreement. For the case of φ=4.9%, and at Re=1284, both computation and experimental results are in excellent agreement. It is noted that when the nanofluid concentration is increased (from φ=0.5% to 4.9%), Nusselt number of numerical computation approaches closer to experimental result. In experiments, for high nanofluid concentrations at low Reynolds number, the fluid pool on the impingement area is effected by the bulk warming, but drainage of the liquid is rather well. There is a continuous fluid film on the impingement surface (heat transfer rate on the surface does not suffer from splashing). In the high Reynolds number range, the fluid splashing effect is dominated and negative effects are more pronounced than positive heat transfer enhancement effect. As a result, both effects eliminate the negative effect of bulk warming and finally numerical and experiment results show a very close agreement to each other in low Reynolds number range. In numerical simulations also, for the φ=4.9%, instantaneous averaged Nusselt number shows little oscillations which can be seen in Fig. 12.

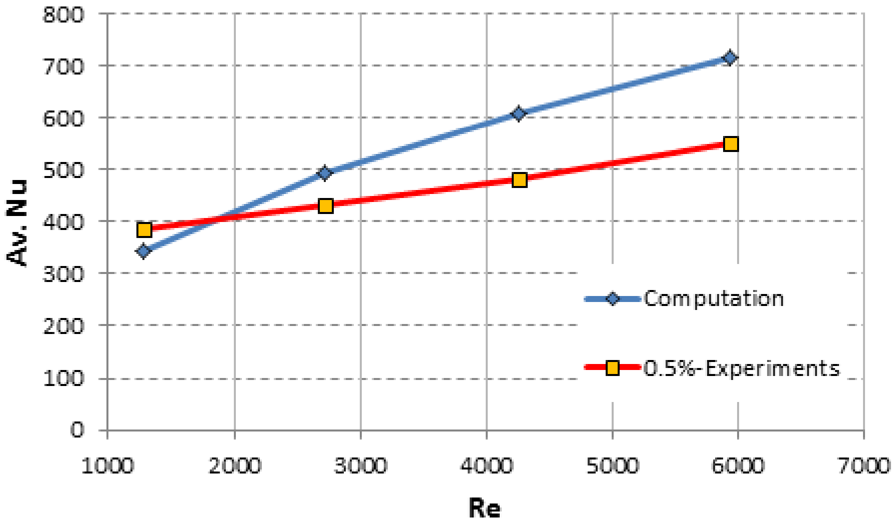

Fig. 9 Numerical Result vs Experimental Result for the case of φ=0.5% Nanofluid . H/dn=12.33, S/dn=7

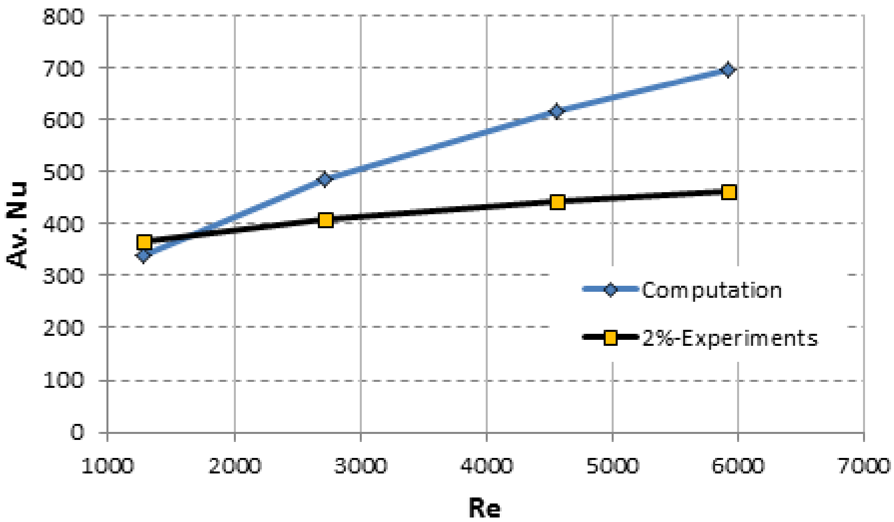

Fig. 10 Numerical Result vs Experimental Result for the case of φ=2% Nanofluid . H/dn=12.33, S/dn=7

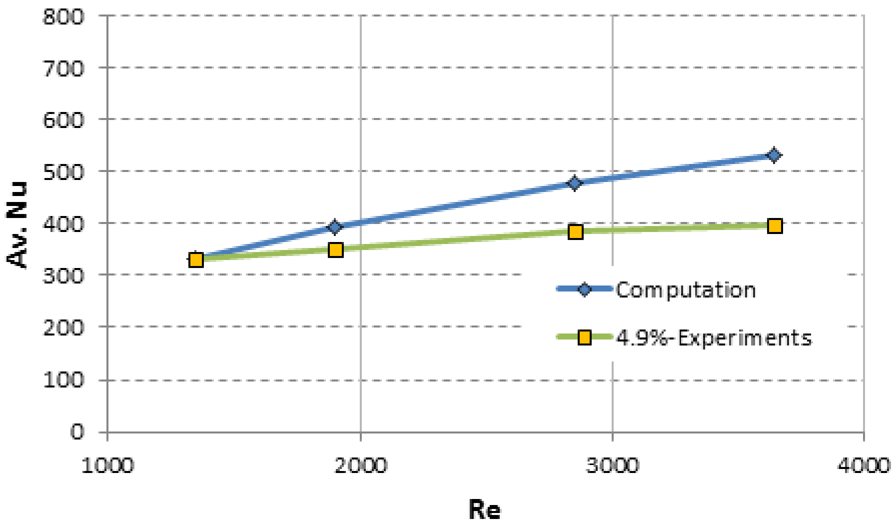

Fig. 11 Numerical Result vs Experimental Result for the case of φ=4.9% Nanofluid . H/dn=12.33, S/dn=7

Both in numerical simulations and in experimental measurements, high fluid velocity (at high Reynolds number) under free surface jet impingement condition has a distortive effect on impinging jet columns. In Fig. 12, recirculation zones formed between two neighboring jets can be clearly observed in numerical simulations. These recirculation zones distort location of stagnation point of impinging jets and decreases fluid film thickness on the surface. Also, as the growing fluid pool on the impingement surface is captured by high speed video camera as seen in previous figure, this pool causes a fountain flow towards nozzle orifice plate and this fountain flow significantly affects impinging jet columns and causes heat transfer reduction on the impingement surface as illustrated in Fig. 13. One of the reasons why a discrepancy is observed between numerical and experimental results in high Reynolds number range, is this jet column deterioration by recirculation zones and fountain flows because these phenomena are very unsteady and chaotic that is very difficult to predict in simulations.

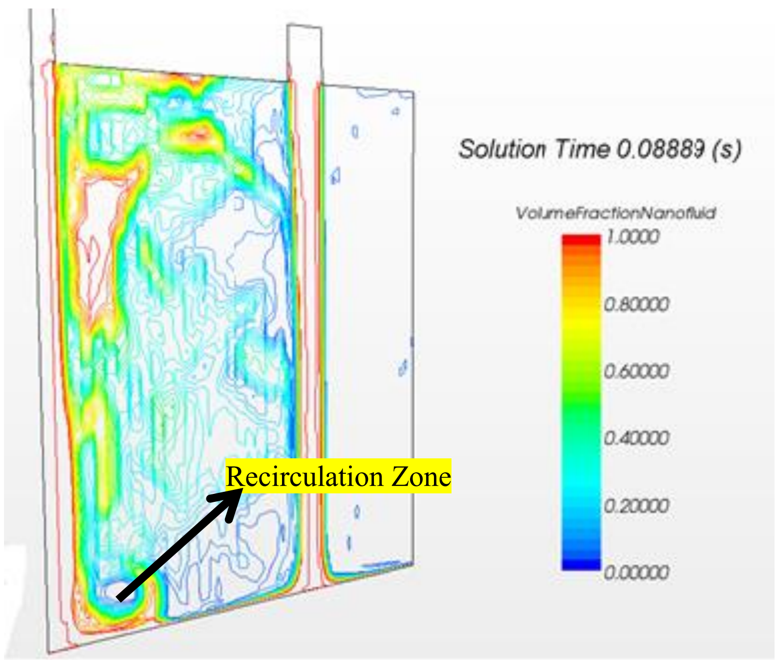

Fig. 12 Volume Fraction contours of φ=4.9% suspension at Re=3639 (Intermediate-High Reynolds number range). Recirculation zone is formed near the impingement zone

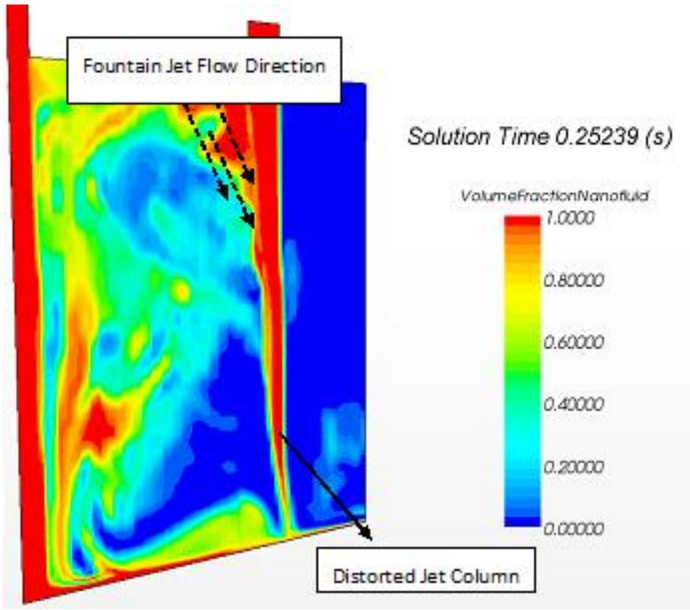

Fig. 13 Jet column distortion due to the fountain jet (φ=4.9%, Re=3639)

5 Summary

An experimental and numerical investigation has been carried out to have a better understanding of the physical mechanisms associated with nanofluid jet array. Main effort was made to investigate nanofluid jet array impingement phenomenon. Target impingement surface average heat transfer coefficient was determined. Comparisons are made according to available free jet array data. A complete data set is generated from the experimental measurements and numerical predictions both for nanofluid jet array impingement. Higher particle volume fractions of Al_2O_3–Water nanofluid exhibit unfavorable heat transfer characteristics under array formation.

References

[1] Whelan B. P, Kempers R, Robinson A. J (2012) A liquid-based system for CPU cooling implementing a jet array impingement water block and a tube array remote heat exchanger. *Appl. Therm. Eng*., vol. 39, pp. 86–94.

[2] Chien L.-H, Chang C.-Y (2011) An experimental study of two-phase multiple jet cooling on finned surfaces using a dielectric fluid. *Appl. Therm. Eng*., vol. 31, no. 11–12, pp. 1983–1993.

[3] Jiji L, Dagan Z (1987) Experimental investigation of single phase multi-jet impingement cooling of an array of microelectronic heat sources. In: Proceedings of the International Symposium on Cooling Technology for Electronic Equipment, pp. 333–335.

[4] Womac D. J, Incropera F. P, Ramadhyani S (1994) Correlating Equations for Impingement Cooling of Small Heat Sources with multiple circular liquid jets. *ASME J. Heat Transfer*, vol. 115, pp. 8–12.

[5] Pan Y, Webb B. W. (1995) Heat Transfer Characteristics of Arrays of Free-Surface Liquid Jets. *ASME J. Heat Transfer*, vol. 117, pp. 878-883.

[6] Robinson A. J, Schnitzler E (2007) An experimental investigation of free and submerged miniature liquid jet array impingement heat transfer. *Exp. Therm. Fluid Sci.*, vol. 32, no. 1, pp. 1–13.

[7] Fabbri M, Dhir V. K (2005) Optimized Heat Transfer for High Power Electronic Cooling Using Arrays of Microjets. *ASME J. Heat Transfer,* vol. 127, no. 7, pp. 760-766.

[8] Tie P, Li Q, Xuan Y. (2011) Investigation on the submerged liquid jet arrays impingement cooling. *Appl.*

Therm. Eng., vol. 31, no. 14, pp. 2757–2763.

[9] Nguyen C. T, Galanis N, Polidori G, Fohanno S, Popa C. V, Le Bechec A. (2009) An experimental study of a confined and submerged impinging jet heat transfer using Al_2O_3-water nanofluid. *Int. J. Therm. Sci.,* vol. 48, no. 2, pp. 401–411.

[10] Xuan Y, Li Q. (2003) Investigation on Convective Heat Transfer and Flow Features of Nanofluids. *ASME J. Heat Transfer*, vol. 125, no. 1, pp. 151-157.

[11] Palm S. J, Roy G, Nguyen C. T. (2006) Heat transfer enhancement with the use of nanofluids in radial flow cooling systems considering temperature-dependent properties. *Appl. Therm. Eng.*, vol. 26, no. 17, pp. 2209–2218.

[12] Feng Y, Kleinstreuer C. (2010) Nanofluid convective heat transfer in a parallel-disk system. *Int. J. Heat Mass Transf.*, vol. 53, no. 21–22, pp. 4619–4628.

[13] Maxwell J. C. (1873) A Treatise on Electricity and Magnetism. Clarendon Press, Cambridge.

[14] Kakaç S. Pramuanjaroenkij A. (2009) Review of convective heat transfer enhancement with nanofluids. *Int. J. Heat Mass Transf.*, vol. 52, no. 13–14, pp. 3187–3196.

[15] Rea U, McKrell T, Hu L, Buongiorno J. (2009) Laminar convective heat transfer and viscous pressure loss of alumina–water and zirconia–water nanofluids. *Int. J. Heat Mass Transf.*, vol. 52, no. 7, pp. 2042–2048.

[16] Batchelor G. K. (1977) The effect of Brownian motion on the bulk stress in a suspension of spherical particles. *Journal of Fluid Mechanics*, vol. 83. pp. 97-105.

[17] Rodi, W. (1982) Examples of Turbulence Models for Incompressible Flows. *AIAA, J.*, vol. 20, pp. 872-879.

[18] Torii S, Shimizu A, Hasegawa S, Higasa M. (1990) Laminarization of Strongly Heated Gas Flows in a Circular Tube (Numerical Analysis by Means of a Modified k-ε Model). *JSME Int. J.,* Ser. II, vol. 33, no. 3, pp. 538-547.

[19] Nagano Y, Hishida M. (1987) Improved form of the k-ε Model for Wall Turbulent Shear Flows. *Trans. of ASME*, Ser. D, vol. 109, pp. 156-160.

[20] Nguyen C. T, Galanis N, Polidori G, Fohanno S, Popa C. V, Le Bechec and A. (2009) Exerimental study of a confined and submerged impinging jet heat transfer using Al_2O_3-water nanofluid. *Int. J. Therm. Sci.*, vol. 48, no. 2, pp. 401–411.